Determination of the standard rate constant for soluble-soluble *quasi*-reversible electrochemical systems by linear sweep voltammetry: Application to the electrochemical oxidation on screen-printed graphite electrodes

Sabrina Houam [a], Abed Mohamed Affoune [a,*], Imene Atek [a], Fatima Kesri [a,b], Rania Saad Guermeche [a], Mohamed Lyamine Chelaghmia [a], Mouna Nacef [a], Omar Khelifi [a,c], Craig E. Banks [d]

[a] *Laboratory of Industrial Analysis and Materials Engineering, University May 8, 1945 Guelma, P.O.B. 401, Guelma 24000, Algeria*

[b] *Department of Chemistry, University Badji Mokhtar-Annaba, Annaba, Algeria*

[c] *Department of Hydrocarbon and Renewable Energy, University Ahmed Draia-Adrar, Adrar, Algeria*

[d] *Faculty of Science and Engineering, Manchester Metropolitan University, Chester Street, Manchester M1 5GD, United Kingdom*

ABSTRACT

Semi-analytical approach was used for modeling and establishing Linear Sweep Voltammetry (LSV) profiles in the case of quasi-reversible electrochemical reactions involving soluble species. The effects of charge transfer coefficient (α) and dimensionless kinetic rate constant (Λ) on the shape and position of voltammograms were investigated. The combined effect on the LSV responses, peak current, half peak width and peak potential was also analyzed qualitatively and quantitatively. Kinetic curves were constructed in the form of the change in the LSV characteristics as a function of (α, Λ) and then modeled by the interpolation functions. The obtained equations are an easy-to-use tool in order to calculate the heterogeneous kinetic rate constant for quasi-reversible charge transfer. Experimental-theory validation has been performed on ferrocyanide oxidation on screen-printed graphite electrodes.

1. Introduction

In electrochemistry, among several electroanalytical techniques to study electrochemical experiments, both linear sweep voltammetry (LSV) and cyclic voltammetry (CV) are often required to study reaction mechanisms as well as for the determination of various thermodynamic and kinetic parameters [1–8]. Modeling and simulation of voltammetry represent an interesting approach for analysing electrochemical processes. They permit an in-depth understanding and obtaining additional information of the experimental curves [9–15]. In this regard, theoretical voltammograms could be calculated using analytical, semi-analytical or digital simulation methods [12].

Using these latter techniques, LSV and CV of electrochemical processes involving a single charge transfer reaction were investigated by several authors. For the systems involving reduced and oxidised soluble species, Randles and Sevcik are the first authors that treated the voltammetric measurement for reversible charge transfer [16,17]. Another important investigation was reported by Nicholson for reversible and irreversible systems [18]. Beside, Matsuda's and Nicholson's works [19,20] are well known for *quasi*-reversible systems. Recently, Samin investigated the effect of adsorption on the voltammetry of these systems [21]. In the case of soluble-insoluble systems, several theoretical studies using various modeling ways for reversible, irreversible and *quasi*-reversible systems were reported by numerous researchers. In this regard Berzins and Delahay are the pioneers in the investigation of modeling voltammograms for reversible systems [22]; Delahay examined the case of totally irreversible systems [23]. For the *quasi*-reversible systems, the first study has been presented by Krulic [24], and recently, a study was presented by Atek [25].

Matsuda has established three diagrams related to the variation of peak current, half peak width and peak potential features of LSV curves as a function of the kinetic rate constant for *quasi*-reversible soluble-soluble systems [19]. These diagrams can allow the experimenter to

Nomenclature

I	current
n	number of electrons
F	Faraday's constant
A	surface area of electrode
D_{Ox}	diffusion coefficient of oxidized species (Ox)
D_{Red}	diffusion coefficient of reduced species (Red)
k^0	standard rate constant
α	anodic charge transfer coefficient
1—α	cathodic charge transfer coefficient
R	universal gas constant
T	absolute temperature
E	electrode potential
E_{eq}	equilibrium potential
E^o	standard potential
E_i	initial potential
v	scan rate
t	time

roughly estimate the kinetic rate constant, but they are still not practical enough for quantitative analysis. For *quasi*-reversible soluble- insoluble reaction, Atek presented, in addition to different diagrams, a series of useful equations that could be used to estimate the kinetic rate constant of studied reactions with good precision and application of the obtained equations has been made on the electroreduction of copper ions [25]. Determination of the standard heterogeneous rate constant k° for the soluble-soluble *quasi*-reversible electrochemical systems by cyclic voltammetry is generally evaluated using the Nicholson method [20] in which peak potential separations are correlated to the k^0. Lavagnini has proposed an empirical relationship between the dimensionless kinetic parameter and peak potential separations which practically replaces the Nicholson's working curve [26]. In another hand, Gonzalez has deduced an equation for the determination of standard rate constants for electrochemical irreversible processes from linear sweep voltammograms [27]. However, and as far as we know, there are no relationships to correlate between linear sweep voltammograms characteristics and electron transfer rate constant k^o for soluble-soluble *quasi*-reversible electrochemical systems.

In this paper, modeling, and calculation of LSV responses for *quasi*-reversible reaction involving soluble species have been carried out by a semi-analytical method with different kinetic curves were constructed. Subsequently, interpolation equations were developed. The validity of the theoretically obtained results was assessed by electrochemical oxidation of ferrocyanide in potassium chloride medium using screen-printed graphite electrode.

2. Modeling and calculation procedures

We consider a simple electron-transfer reaction between reduced (*Red*) and oxidized (*Ox*) soluble species:

$$Red \rightleftarrows Ox + ne^- \tag{1}$$

the Butler-Volmer equation is assumed to describe the latter process:

$$I(t) = nFAk^0\left[C_{red}(0,t)e^{\frac{\alpha nF}{RT}(E-E^0)} - C_{ox}(0,t)e^{\frac{-(1-\alpha)nF}{RT}(E-E^0)}\right] \tag{2}$$

where I, n, F, A, k^0, α, R, T, E, and E^o are defined in the Nomenclature section.

$C_{red}(0,t)$ and $C_{ox}(0,t)$ are respectively the concentration of reduced (Red) and oxidized (Ox) soluble species at the surface of electrode at instant t.

The mass transport of the electroactive species to the electrode surface is considered controlled by diffusion and can be described by Fick's second law:

$$\frac{\partial C(x,t)}{\partial t} = D\frac{\partial^2 C(x,t)}{\partial x^2} \tag{3}$$

by assuming that, initially, only *Red* species are present in the bulk solution, initial and boundary conditions are given below:

$$t = 0,\ x \geq 0,\ C_{Red}(x,0) = C^{\omega}_{Red}, C_{Ox}(x,0) = 0 \tag{4}$$

$$t > 0,\ x \to \infty,\ C_{Red}(\infty,t) = C^{\omega}_{Red},\ C_{Ox}(\infty,t) = 0 \tag{5}$$

$$t > 0,\ x \to 0,\ J_{Red}(0,t) = \frac{I(t)}{nFA} = D_{Red}\left[\frac{\partial C_{Red}(x,t)}{\partial x}\right]_{x=0} \tag{6}$$

where: $J_{Red}(0,t)$ is the flux of *Red* species at the electrode surface ($x = 0$).

The concentration at the electrode surface $C(0, t)$ of *Red* and *Ox* species as function of the time, could be obtained analytically using Laplace's transform under conditions of Eqs. (4)–(6). The solution was expressed as [9]:

$$C_{Red}(0,t) = C^{\omega}_{Red} - \frac{1}{nFA\sqrt{\pi D_{Red}}}\int_0^t \frac{I(\tau)}{\sqrt{t-\tau}}d\tau \tag{7}$$

$$C_{Ox}(0,t) = \frac{1}{nFA\sqrt{\pi D_{Ox}}}\int_0^t \frac{I(\tau)}{\sqrt{t-\tau}}d\tau \tag{8}$$

In linear sweep voltammetry, the potential E is linearly scanned at any time t with a constant scan rate *v* starting from an initial potential E_i:

$$E = E_i + vt \tag{9}$$

The initial state is supposed to be at the equilibrium state; hence the initial potential E_i obeys to the Nernst Equation:

$$E_i = E_{eq} = E^0 + \frac{RT}{nF}ln\left(\frac{C^{\omega}_{Ox}}{C^{\omega}_{Red}}\right) \tag{10}$$

by combination of the Eqs. (2), (7)–(10), we obtain the general current *I* equation as follows:

$$I(t) = nFA\ C^{\omega}_{Red}(D_{Red})^{1/2}\left(\frac{nF}{RT}\right)^{1/2}v^{1/2}\pi^{1/2}\ \mathbf{X}(\sigma t) \tag{11}$$

The dimensionless current $\mathbf{X}(\sigma t)$ is given by the following integral:

$$\int_0^{\sigma t}\frac{\mathbf{X}(z)}{\sqrt{\sigma t - z}}dz = \left[\frac{1}{1+[\theta S(\sigma t)]^{-(\alpha+\beta)}}\right]\left[1 - \mathbf{X}(\sigma t)\frac{\sqrt{\pi}}{\Lambda}[\theta S(\sigma t)]^{-\alpha}\right] \tag{12}$$

where:

$$\sigma = \frac{nFv}{RT} \tag{13}$$

$$S(\sigma t) = exp(\sigma t) \tag{14}$$

$$\theta = \exp\left(\frac{nF}{RT}(E_i - E^0)\right) \tag{15}$$

$$\Lambda = \frac{k^0}{\sqrt{\sigma D_{Red}}} \tag{16}$$

Λ is called the dimensionless rate constant.

The calculation of the integral in the expression (12) was obtained using the numerical method developed by Nicholson and Shain [20] which leads to the following algorithm:

$$\chi(1)\sqrt{N} + \sum_{i=1}^{N-1}\sqrt{N-i}\,[\chi(i+1)-\chi(i)]\left[\frac{1}{1+[\theta S(\delta N)]^{-(\alpha+\beta)}}\right]\left[1-\mathbf{X}(\delta N)\sqrt{\frac{\delta}{\Lambda}}[\theta S(\delta N)]^{-\alpha}\right] = 2\sqrt{\delta} \tag{17}$$

where δ is the calculation step.

While the dimensionless current is noted $\mathbf{X}(\sigma t)$, the dimensionless potential is noted Pot(σt). Its expression is as follows:

$$Pot(\sigma t) = \Phi = \frac{nF}{RT}(E - E^{0}) = init + \sigma t \tag{18}$$

At, $t = 0$, $Pot(0) = init = \frac{nF}{RT}(E_{init} - E^{0})$ (19)

E_{init} is the dimensionless initial potential, at which the dimensionless current is zero.

By giving values of δ, *init*,Φ, Λ and α in this algorithm, the dimensionless LS voltammograms can be calculated and the general form of the solution of Eq. (17) is a set of values of $\mathbf{X}(\sigma t)$ as a function of $Pot(\sigma t)$.

3. Calculation and experimental tools

3.1. Calculation methods

The simulation programs were coded in Fortran 90 and compiled with the Microsoft Fortran PowerStation 4.0. Data analysis and graphing were performed with Origin 2018. Tafel plots were used to calculate the charge transfer coefficient. Semi-integration (SI) technique was applied in order to calculate diffusion coefficient through the algorithm developed by Oldham [28,29].

3.2. Experimental tools

3.2.1. Reagents

Reagents grade potassium ferrocyanide $K_4(FeCN_6)$ (99%) and potassium chloride KCl (99%) were purchased from Sigma-Aldrich Company. All reagents were used without purification and all solutions were prepared with deionized water.

3.2.2. Instrumentation and procedure

The LSV voltammetric measurements were performed with a VersaSTAT 3 Potentiostat (Princeton Applied Research, AMETEK, USA) controlled by Versa Studio software. All electrochemical experiments were conducted in a single-compartment cell at room temperature in which a screen-printed graphite electrode (SPE) from Manchester Micropolitan University was used without preparation. The SPE consisted of a graphite working electrode (0.0707 cm^2), a graphite counter electrode, and an Ag/AgCl reference electrode. All experiments were carried out in potassium ferrocyanide (5 mM) with KCl (0.1 M) supporting electrolyte. The potential was typically scanned from to -400 mV to 800 mV *vs*. Ag/AgCl at scan rates ranging between 30 and 200 mV s^{-1}.

4. Results and discussion

4.1. Theoretical results

In LSV, the magnitudes of the peak current, half peak width, and peak potential are the most commonly parameters used for evaluating the characteristics of electron transfer process. The main factors affecting the voltammogram features are the charge transfer coefficient α and the heterogeneous standard rate constant k^0. The combined influence of k^0 and v is expressed through the dimensionless kinetic parameter, Λ, given by Eq. (16). The effects of varying Λ and α on the peak current amplitude, the peak potential, and the half peak width are examined in this section.

A typical theoretical linear sweep voltammetric responses of a reversible system calculated at $\Lambda=10^3$ and $\alpha=0.5$ with two different, cathodic and anodic, sweep potential directions are presented in Fig. 1. The voltammograms are symmetric and both show the identical features regarding shape and the absolute values of peak current. Hence, the direction of the potential sweep has no effect on the characteristics of voltammograms of soluble-soluble systems.

4.1.1. Effect of kinetic rate

At a constant value of charge transfer coefficient, the effect of varying the dimensionless kinetic parameter Λ on the voltammograms characteristics was investigated. An example for the evolution of dimensionless peak current values versus those of dimensionless rate constant at $\alpha = 0.5$ is presented in Table 1. The voltammogram curves for different values of α are presented in Fig. 2 in which we have limited the range of Λ so as not to clutter the figures too much. Analysis of the data show that three regions could be distinguished:

1) $\wedge \geq 10^3$

In this region, the dimensionless peak current $\pi^{1/2}\chi_p$ remains constant at 0.4463. This value is identical to those of literature results related to the case of reversible soluble-soluble systems [16–18].

2) $\wedge \leq 10^{-3}$

In this region, the dimensionless current-potential curves have similar shapes while the peak potential shifts to anodic values as ∧ decreases. The dimensionless peak current keeps constant at $\pi^{1/2}\chi_p = 0.4958\ \alpha^{1/2}$ .This value was reported previously for irreversible charge transfer reaction [18].

3)$10^{-3} < \wedge < 10^3$

In this intermediate region, the peak features are closely dependent on the dimensionless rate constant ∧. Hence, the decrease of ∧ leads to a decrease of $\pi^{1/2}\chi_p$. The peak potential shifts slightly to anodic values, as ∧ decreases. Because this region is situated between both limited regions of reversible and irreversible charge transfer reactions as indicated above, it is identified that it corresponds to the *quasi*-reversible systems [19,20,25].

4.1.2. Effect of the charge transfer coefficient

Fig. 3 shows a series of linear sweep voltammograms calculated for a variety of charge transfer coefficient α at different dimensionless rate constant ∧. Results indicated that for $\Lambda = 10^3$, there is no effect of charge transfer coefficient on the voltammograms. For Λ≤1 and $\Lambda = 10^{-1}$, peak current vary as α increases. However, the curves are not totally separated, i.e., they partially overlap, whatever the α value. For

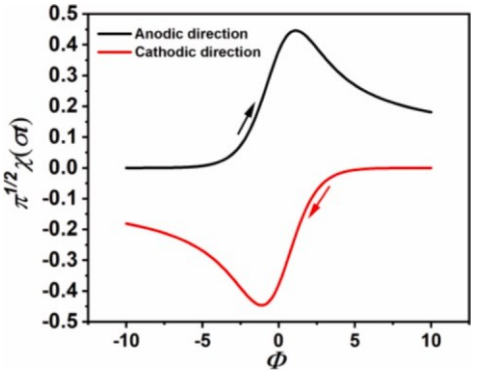

Fig. 1. Theoretical linear sweep voltammetry profile for reversible soluble-soluble reaction with anodic (black) and cathodic (red) sweep potential directions

Table 1
Dimensionless rate constant $\wedge$ and dimensionless peak current $\pi^{1/2}\mathbf{X}_p$ for different curves presented in Fig. 2b.

$\wedge$	$\pi^{1/2}\mathbf{X}_p$	$\wedge$	$\pi^{1/2}\mathbf{X}_p$	$\wedge$	$\pi^{1/2}\mathbf{X}_p$
10^6	0.4463	10^2	0.44575	10^{-3}	0.3505
10^5	0.4463	10^1	0.4410	10^{-4}	0.3505
10^4	0.4463	10^0	0.4069	10^{-5}	0.3505
10^3	0.44625	10^{-1}	0.3559	10^{-6}	0.3505
		10^{-2}	0.3507		

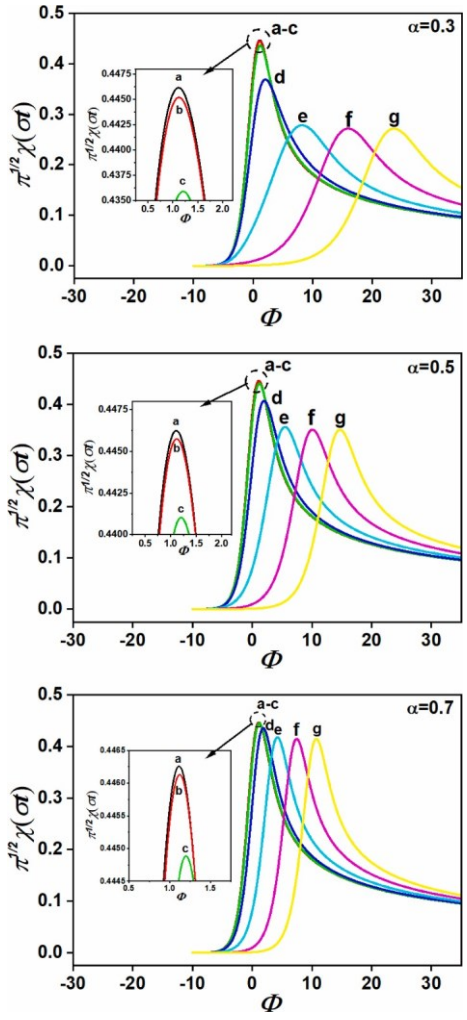

Fig. 2. LSVs responses calculated for various value of $\wedge$ with $\boldsymbol{\alpha}$=0.3 (top), 0.5 (middle) and 0.7 (bottom) a) $\wedge = 10^3$, b) $\wedge = 10^2$, c) $\wedge = 10^1$, d) $\wedge = 1$, e) $\wedge = 10^{-1}$, f) $\wedge = 10^{-2}$, g) $\wedge = 10^{-3}$,

$\Lambda = 10^{-3}$, both peak current and peak potential are dependent on the charge transfer coefficient. When α increases the peak current increases, peak potential shifts to anodic values and voltammograms are totally separated. The deduced conclusions from these examples corroborate with those presented in Section 4.1.1.

From results in Figs. 2 and 3, it is clear that both the dimensionless kinetic rate Λ and the charge transfer coefficient α have a combined effect on the features of the linear sweep voltammograms and consequently peak parameters may change as a function of Λ and α.

4.1.3. Kinetics curves and interpolation equations

Kinetic curves. Matsuda and Ayabe have already investigated the effect of Λ and α on peak parameters and established three diagrams related to

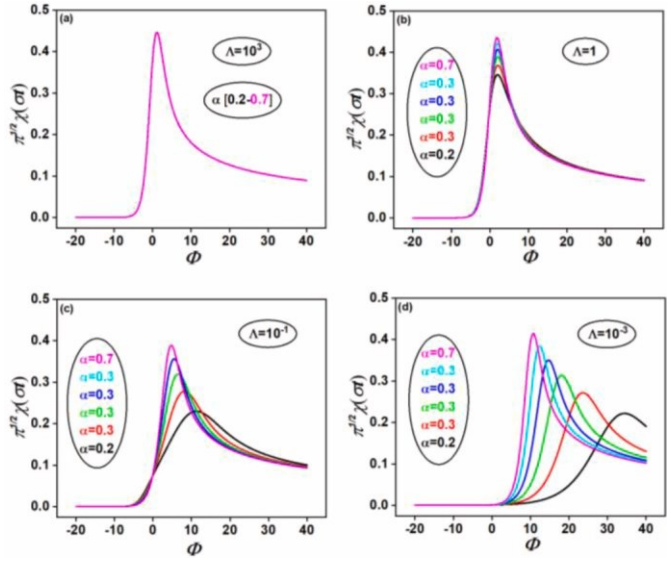

Fig. 3. Effect of charge transfer coefficient on voltammograms at different values of Λ: (a) $\Lambda=10^3$, (b) $\Lambda=1$, (c) $\Lambda=10^{-1}$, (d) $\Lambda=10^{-3}$

the dimensionless peak current, the half peak width and the peak potential as a function of the normalized heterogeneous rate constant Λ and the electron transfer coefficient α [20]. In this section, we have first rebuilt the three Matsuda's diagrams in the ranges of $\wedge = [10^{-6} - 10^{6}]$ and $\alpha = [0.2 - 0.7]$. Then, from these latter's, four new diagrams were extracted for specified Λ ranges. Subsequently, interpolation was used to establish different characteristic equations to be used for determination of standard rate constant from experimental voltammograms, especially, in the case of *quasi*-reversible systems.

Fig. 4 shows different peak characteristics as a function of $log\wedge$ and α. It displays the plots of the peak current ratio $\Psi_p/(\Psi_p)_{rev} = \pi^{1/2}\chi_p/(\pi^{1/2}\chi_p)_{rev}$, the half peak width $\Delta\Phi_{p/2} = \frac{nF}{RT}(E_p - E_{p/2})$ and the peak potential $\eta_p = \frac{nF}{RT}(E_p - E^o)$ versus log (Λ) and α. 2D presentation is on the left side of Fig. 4 while 3D presentation is on the right side. $(\Psi_p)_{rev}$ is the reversible dimensionless peak current and equals to 0.4463. At first glance, it can be concluded that the observed features are similar to those reported by Matsuda. The first two series of curves have a sigmoidal dependency. However, the last series has a quadratic dependency. The 3D diagrams show more clearly the separation between the different zones than in 2D diagrams. The transition from a reversible system to an irreversible one is better defined. Fig. 5 illustrates the linear parts of the curves presented in Fig. 4. This simplified presentation allows us to obtain easily a linear interpolation in the selected ranges of $\wedge$.

Although the shape of the curves in Fig. 4 are significantly different, the agreement between them can be determined in three well distinct kinetic zones which are as follows:

Zone A: It covers the region where $\wedge \geq 10^{+3}$. In this zone there is no influence of the dimensionless kinetic rate $\wedge$ and α on the peak parameters. The expressions of the current peak, the half peak width and the potential peak are the same of that of the reversible charge transfer reaction [16–18,30].

$$I_p = 0.4463\ n\ F\ AC^{\omega}_{Red}(D_{Red})^{1/2}\left(\frac{nF}{RT}\right)^{1/2}\nu^{1/2} \quad (20)$$

$$E_p - E_{p/2} = 2.20\frac{RT}{nF} \quad (21)$$

$$E_p = E_{1/2} - 1.109\frac{RT}{nF} \quad (22)$$

Zone B: It is in the range of $(10^{-3} < \wedge < 10^{3})$ which exhibits *quasi*-

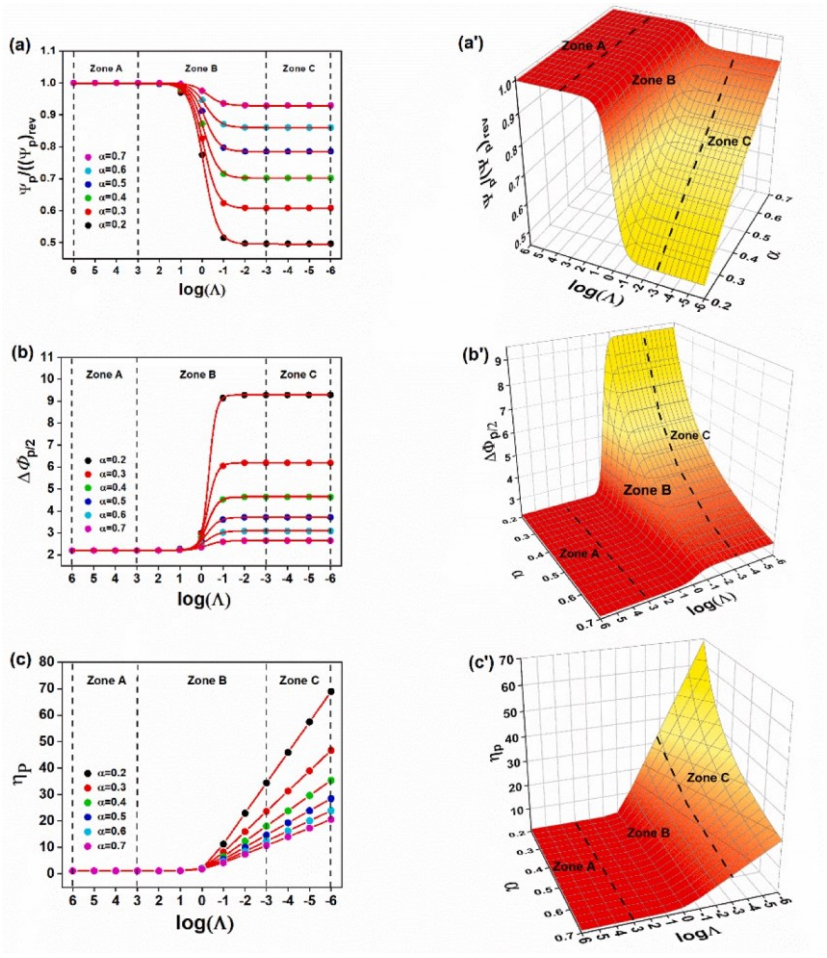

Fig 4. 2D (left) and 3D (right) presentation of the effect of the kinetic rate constant Λ and charge transfer coefficient α on the peak current ratio$\Psi_p/(\Psi_p)_{rev}(a,\ a')$, the half peak width $\Delta\Phi_{p/2}(b,\ b')$, and the peak potential η_p (c, c').

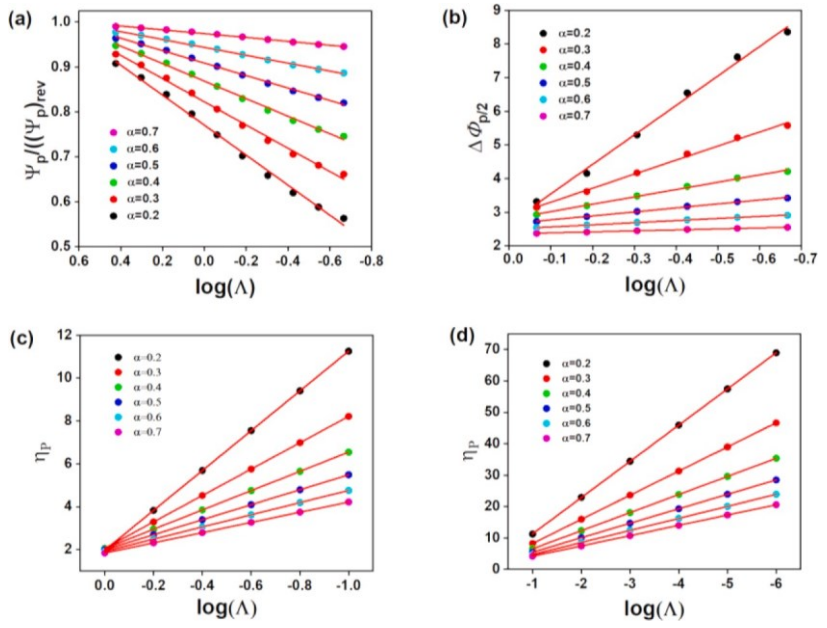

Fig. 5. Linear dependencies of the peak current ratio$\Psi_p/(\Psi_p)_{rev}(a)$, the half peak width $\Delta\Phi_{p/2}(b)$, and the peak potential η_p (c, d) on the limiting range of Λ for various α values.

reversible behavior. It could be seen that there was a considerable change in peak characteristics in function of Λ and α. As far as we know, there is no specific kinetics equations identified for this *quasi*-reversible behavior.

Zone C: When $\Lambda \leq 10^{-3}$, the irreversible characteristics are observed in this zone of the curves. For a constant value of α, the peak current and the half peak width are unchangeable as Λ decreases, while the peak potential continues to increase. The known equations related to the irreversible systems [18] could be obtained:

$$I_p = 0.4958\ nF\ A\ C^{\omega}_{Red}(D_{Red})^{1/2}\alpha^{1/2}\left(\frac{nF}{RT}\right)^{1/2}\nu^{1/2} \quad (23)$$

$$E_p - E_{p/2} = 1.857\frac{RT}{nF\alpha} \quad (24)$$

$$E_p = E^0 - \frac{RT}{nF\alpha}\left(0.780 + ln\sqrt{\frac{\alpha nF}{RT}} - \ln k^0\right) \quad (25)$$

Interpolation equations. The diagrams of Fig. 4 a and b show sigmoidal dependencies. The interpolation of the data was fitted perfectly by the sigmoidal Boltzmann function:

$$y = A2 + \left\{\frac{[A1 - A2]}{\left[1 + \exp^{\frac{x-x0}{dx}}\right]}\right\} \quad (26)$$

Where A1, A2, x0 and dx are characteristics of a sigmoid Boltzmann function.

Hence, the following equations were obtained:

$$\frac{\Psi_p}{\Psi_{p\ rev}} = 0.999 + \frac{(1.112\alpha^{0.5} - 0.999)}{1 + \exp\frac{\log(\Lambda) - (-0.489\alpha^3 - 0.0599)}{0.111\alpha^3 + 0.322}} \quad (27)$$

$$\Delta\Phi_{p/2} = 2.214 + \frac{(1.859\alpha^{-1} - 2.214)}{1 + \exp\left(\left[\frac{\log(\Lambda) - (-0.208\alpha^{-0.327})}{0.440\alpha^{0.608}}\right]\right)} \quad (28)$$

The R^2 of Eqs. (27) and (28) are 0.99980 and 0.99988, respectively These fitted equations enable quantification of the electrode kinetics from simple peak current, peak potential and half-peak potential measurements of the experimental linear sweep voltammograms of either reversible, *quasi* reversible or totally irreversible electron transfer process, while α value is known.

Eqs. (27) and (28) are longs and somehow complicated. However, the curves of Fig. 4a in the regions of $log\ \Lambda = [-0.66, 0.42]$ and those of Fig 4b in the region $log\ \Lambda = [-0.66, -0.06]$ have a linear shape as presented in Fig. 5. Data in these two regions of Λ were fitted and the following equations were obtained:

$$\frac{\Psi_p}{\Psi_{p\ rev}} = 1.039\alpha^{0.19} + (0.436 - 0.578\alpha)\log(\Lambda) \quad (29)$$

$$\Delta\Phi_{p/2} = (3.401 - 1.493\alpha) + (3.481 - 2.392\alpha^{-1})\log(\Lambda) \quad (30)$$

The R^2 of Eqs. (29) and (30) are 0.99436 and 0.99912, respectively.

Finally, it is not possible to obtain a simple fit for plots of Fig. 4c in the whole region of Λ. Nevertheless, the following approximate formulas describe linearly the variations of dimensionless peak potential η_p with Λ and α:

When $-1 \geq \log\Lambda \leq 0$,

$$\eta^{o}_{P} = (2.379\alpha^{-0.694}) + (-1.288\alpha^{-0.999})\log(\Lambda) \quad (31)$$

When $\log\Lambda \leq -1$,

$$\eta^{o}_{P} = (1.222 - 0.189\alpha^{-1}) + (-2.296\alpha^{-1})\log(\Lambda) \quad (32)$$

The R^2 of Eqs. (31) and (32) is 0.99833

The obtained Eqs. (27), (28) and (32) have similarity forms with those obtained by Atek et al. [25] for *quasi*-reversible soluble-insoluble systems. Eqs. (29) and (30) are comparable to those obtained by Krulic [24] for staircase voltammetry. The use of these equations is significantly convenient and more accurate than the use of Matsuda diagrams. Furthermore, Matsuda's diagrams were established for only certain values of α, hence it is difficult to estimate constant rate kinetics for intermediate values, we cite as examples the cases when $\alpha = 0.22$ or $\alpha = 0.57$, because the effect of alpha on voltammogram characteristics (Peak current, half peak width and peak potential) is not linear.

4.2. Theory-experiment validation

Experimental cyclic voltammograms, as well as linear sweep voltammograms related to the oxidation of ferrocyanide at screen-printer electrodes (SPE) electrode in KCl electrolyte with different scan rates are presented in Fig. 6a and 6b. The Ferrocyanide/Ferricyanide redox reaction is one of the most commonly well-researched systems in electrochemistry [31–34].

This system is a simple one electron transfer reaction involving soluble species and is described by the following reaction:

$$Fe(CN)^{4-}_6 \rightleftharpoons Fe(CN)^{3-}_6 + 1\ e^-$$

Fig. 6b, shows typically cyclic voltammetric experiments where that as the scan rate increases the peak current increases. Furthermore, the peak potential shifts to anodic values as scan rate increases indicating that the charge transfer is not reversible. The current peaks are linearly proportional to the square root of scan rate as indicated in Fig. 6c suggesting that the electrocatalytic oxidation of $Fe(CN)^{4-}_6$ on SPE was a diffusion-controlled process.

In what follows, we will present in detail the calculation for the voltammogram obtained at 50 mV s^{-1}. Then we present the main results for the other scan rates.

4.2.1. Charge transfer coefficient and diffusion coefficient determination

Fig. 7a illustrates the representation of the Tafel plot obtained from experimental LSV data, at a scan rate of 50 mVs^{-1}. Using the anodic slope of Tafel plots, the value of α equal to 0.259 was calculated and the result is reported in Table 2. The voltammogram of Fig 7a was alternatively analyzed with the semi-integral method. The voltammogram with the corresponding semi-integral curve *m* were presented in Fig 7b. The semi-integral values tend towards a limit, m^*, because the mass transfer is limited by diffusion. The diffusion coefficient $D_{Fe(CN)^{4-}_6}$ could be calculated from this limiting value using the following relationship [28,29]:

$$m^{\omega} = nF\ A\ C^{\omega}_{Red}(D_{Red})^{1/2} \quad (33)$$

The obtained value of $D_{Fe(CN)^{4-}_6}$ is equal to $6.45 \times 10^{-6}\ cm^2\ s^{-1}$. The literature indicated that diffusion coefficient $D_{Fe(CN)^{4-}}$ is in the range reported between 6.10×10^{-6} and $8.0 \times 10^{-6}\ cm^2\ s^{-1}$ [6] in aqueous media [32,35–37].

4.2.2. Standard rate constant determination using interpolation equations

The peak current *Ip*, the peak potential *Ep* and the half peak potential $Ep - E_{p/2}$ of the LS voltammogram in Fig 7a are 0.0325 mA, 0.3828 V and 0.1613 V respectively. These values have to be converted to their dimensionless values. Hence, we found:

$$\frac{\Psi_p}{\Psi_{p\ rev}} = \frac{Ip}{0.4463nFA\ C^{\omega}_{Red}(D_{Red})^{1/2}\left(\frac{nF}{RT}\right)^{1/2}v^{1/2}} = 0.603 \quad (34)$$

$$\Delta\Phi_{p/2} = \frac{nF}{RT}(E_p - E_{p/2}) = 6.278 \quad (35)$$

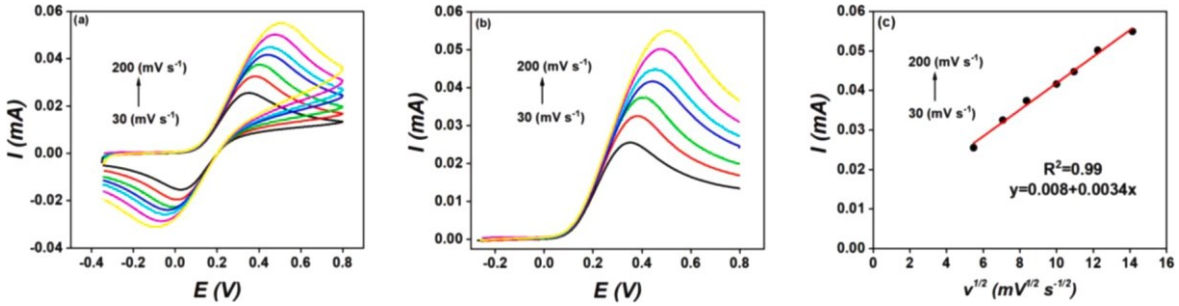

Fig. 6. CV(a) and LSV (b) curves of the oxidation of 5 mM potassium ferrocyanide on screen-printed graphite electrode in the presence of 0.1 M potassium chloride for different scan rates. Variation of the anodic peak currents with the square root of the scan rate (c).

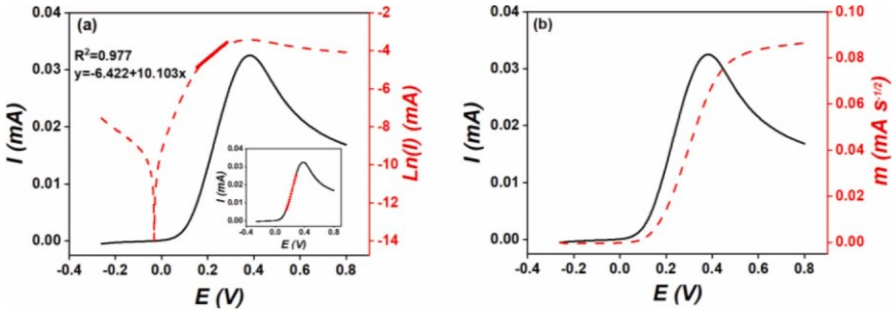

Fig. 7. (a) Tafel plots (dashed red line) and LSV curve (black line) at scan rate of 50 mV s^{-1} (b) LSV response at scan rate of 50 mV s^{-1} (black line), with its convoluted curve (dashed red line).

Table 2
Electrochemical kinetics parameters for ferrocyanide oxidation reaction obtained from the voltammogram recorded at scan rate of 50 mV s^{-1}.

α		$D_{Fe(CN)_6^{-4}}$, 10^{-6} cm^2 s^{-1}		Λ		k^0, 10^{-4} cm s^{-1}	
Tafel	0.259	**SI**	6.45	Eq. (27)	0.1464	Eq. (27)	5.1854
Fit	0.260	**Fit**	6.50	Eq. (28)	0.2426	Eq. (28)	8.5956
				Eq. (29)	0.1987	Eq. (29)	7.0414
				Eq. (30)	0.2709	Eq. (30)	9.5988
				Eq. (31)	0.1866	Eq. (31)	6.6115
				Eq. (32)	0.0916	Eq. (32)	3.2444
				Fit	0.1646	**Fit**	5.8543

$$\eta_p = \frac{nF}{RT}\left(E_p - E^{0}\right) = \frac{nF}{RT}(0.3828 - 0.1337) = 9.696 \quad (36)$$

The value E^o used in this calculation is 0.1337 V [38].

The Eqs. (27)-(32) allow the calculation of the dimensionless rate constant Λ. By using the Eq. (16), we obtain the values of standard rate constant k^0. The results are reported in Table 2.

First, we observe that the values of Λ, situated between 0.09 and 0.24, are in the range of a *quasi*-reversible zone defined in Section 4.1.3 ($10^{-3} < \Lambda < 10^{3}$) and also in the range that proposed by Matsuda ($10^{-2}{}^{(1+\alpha)} < \Lambda < 15$) [19] and Kwak ($10^{-1.7} < \Lambda < 10^{1.7}$) [39]. The literature indicated that k^0 values of ferrocyanide oxidation reaction is in the range between 4.9×10^{-4} and 2.0×10^{-2} cm s^{-1} [40,41] on the carbon material electrodes. The values calculated, herein, are in this range and indicate that the behavior of ferrocyanide on screen-printed graphite electrode is *quasi*-reversible. The main important point here is to show a more interesting and easier way to determine rate constant from the characteristic points of linear sweep voltammetry curves.

4.2.3. Simulation and fitting

We demonstrate in what follows the applicability of the developed equations. On this basis, we have first simulated the voltammograms using the values of D, α and k^0 as obtained in Sections 4.2.1 and 4.2.2. Furthermore, we proceeded to the fitting test in which we used various values of D, α and k^0 to achieve the best fit between the calculated and experimental curves.

The simulated voltammograms are presented in Fig. 8. It can be observed that the voltammograms obtained using k^0 of Eqs. (27)-(32) have a good agreement and are very close to the experimental voltammogram especially those obtained by using Eqs. (27), (29) and (31) related to the peak current and peak potential. The small discrepancies using equations 28 and 30 could be attributed to effect of ohmic drop, however for that using Eq. (32) could be attributed to the dimensionless rate constant Λ which was out of range of applicability of this equation.

An excellent fit (Fig. 9) was reproduced between the experimental LSV and a simulated one with the following parameters:

$D = 6.5 \times 10^{-6}$ cm^2 s^{-1}, $\alpha = 0.26$ and $k^0 = 5.8543 \times 10^{-4}$ cm s^{-1}.

The k^o value obtained by fitting is in the range of k^0 values calculated by Eqs. (27)-(32). It is particularly close to the values calculated by Eqs. (27), (29) and (31).

In Fig. 9, we compared the fitted curve, the experimental voltammogram and the simulated voltammogram calculated using the mean value of k^0 equals to 6.7129×10^{-4} cm s^{-1}. The three curves are very close indicating that the mean value of k° could be used to overcome the small discrepancies between the different values of k° calculated by the different Eqs. (27)-(32).

The same procedure was employed to analyse the voltammograms obtained at different scan rates. In Table 3, we summarised the different k^0 values obtained using different equations for each scan rate. Excellent fits were reproduced between the experimental LSVs and simulated ones under various scan rates as shown in Fig. 10. The simulated voltammograms were calculated using mean value of k° for each scan rate. These results confirm the above conclusions and reveal that the interpolation functions provided in this work could be used to analyse successfully the experimental linear sweep voltammograms for *quasi*-reversible soluble/soluble systems.

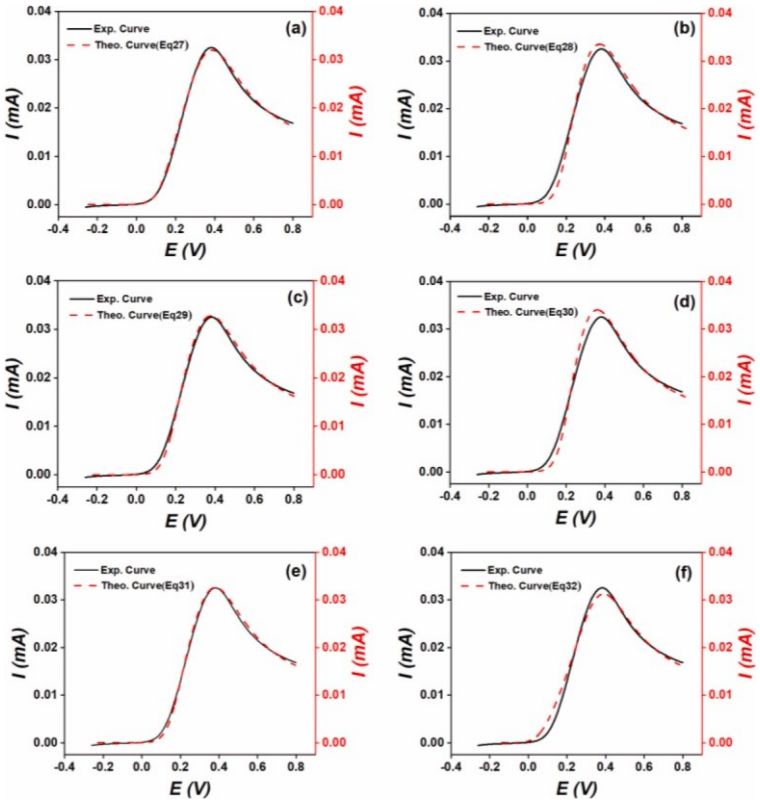

Fig. 8. Comparison between theoretical LSV curves obtained by using k^0 of Eqs. (27)–(32) to experimental voltammogram recorded at a scan rate 50 mV s^{-1}.

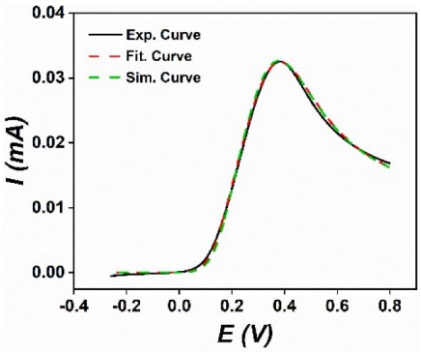

Fig. 9. Comparison between experimental, fitted and simulated voltammograms. The simulated voltammogram was calculated using the mean value of k^0.

5. Conclusions

Modelling and calculation of voltammograms related to *quasi*-reversible soluble/soluble systems have been done using semi-analytical method. The effects of charge transfer coefficient and kinetic rate constant on the shape and position of voltammograms were investigated. Qualitative and quantitative analysis of combined effects of charge transfer coefficient and kinetic constant rate on the main features of LSV voltammograms, *i.e.*, peak current, half peak width and peak potential were established. Kinetic curves and their interpolation functions were presented. The applicability of the obtained equations enables the determination of kinetic rate constant for *quasi*-reversible soluble/soluble systems. Experimental-theory validation has been performed on ferrocyanide oxidation on screen printed graphite electrodes. The value of k^0 was calculated easily using the developed equations. Almost all the equations we established could be used to determine the kinetic rate constant without restriction of reversibility of the investigated system. Since the limits between reversible and *quasi*-reversible or irreversible and *quasi*-reversible are not well defined, our equations are valid for all the spectra of rate constants. Of course, when the kinetics of a system is well characterised as totally reversible or totally irreversible, the classical equations should be applied.

Table 3
Electrochemical standard rate constant k° for ferrocyanide oxidation reaction obtained from the voltammogram recorded at different scan rates.

v mV s^{-1}	k^0, 10^{-4} cm s^{-1}							
	Eq. (27)	Eq. (28)	Eq. (29)	Eq. (30)	Eq. (31)	Eq. (32)	Mean value of k^0	fit
20	4.0005	12.0914	4.8449	8.1107	9.8435	3.2714	7.0271	4.2575
30	4.6203	9.1586	5.7654	9.6403	9.0564	3.4565	6.9496	4.9075
50	5.1854	8.5956	7.0414	9.5988	6.6115	3.2444	6.7129	5.8543
70	5.1462	9.2838	7.8476	10.6512	6.2719	3.4123	7.1022	5.3640
100	4.9108	10.5391	8.7916	12.0350	6.3537	3.8051	7.7393	6.2153
120	3.5750	8.0777	8.9398	11.4859	5.5540	3.6733	6.8843	6.5343
150	6.5218	9.6474	10.9634	12.9617	5.4971	3.8707	8.2437	8.2779
200	2.6182	6.5977	10.8614	13.6003	5.2846	4.0730	7.1725	6.9932

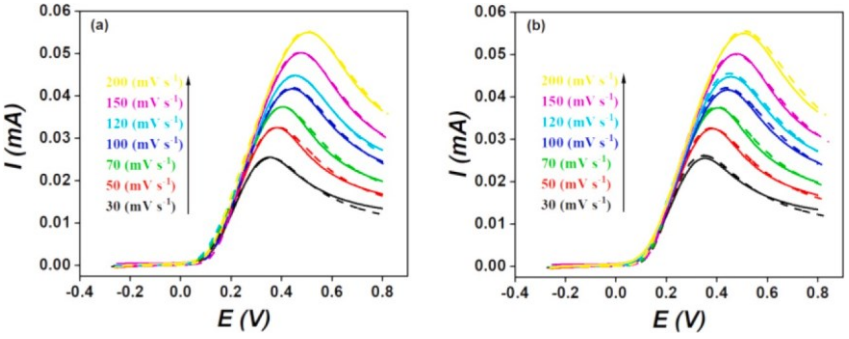

Fig. 10. Fitted (dashed curves, (a) and simulated (dashed curves, (b) voltammograms compared to experimental voltammograms (solid curves) at different scan rates.

Declaration of Competing Interest

The authors declare that they have no known competing financial interests or personal relationships that could have appeared to influence the work reported in this paper.

Data availability

No data was used for the research described in the article.

Acknowledgments

The authors acknowledge the financial support offered by the General Direction of Scientific Research and Technology Development, the Algerian Ministry of Higher Education and Scientific Research, Algeria.

References

[1] T. Gueshi, K. Tokuda, H. Matsuda, Voltammetry at partially covered electrodes Part II. Linear potential sweep and cyclic voltammetry, J. Electroanal. Chem. 101 (1979) 29–38.
[2] J. Gonzalez-Velasco, The linear sweep voltametric method: an application to the study of reversible and irreversible processes, Electroanalysis 6 (1994) 711–724.
[3] J. Heinze, Theory of cyclic voltammetry at microdisk electrodes, Ber. Bunsenges. Phys. Chem. 85 (1981) 1096–1103.
[4] F. Lantelme, E. Cherrat, Application of cyclic voltammetry to the study of diffusion and metalliding processes, J. Electroanal. Chem. 244 (1988) 61–68.
[5] C.A. Basha, M.V. Sangaranarayanan, On the evaluation of the current function in linear sweep voltammetry, J. Electroanal. Chem. 261 (1989) 431–436.
[6] T. Suzuki, I. Mori, H. Nagamoto, M.M. Ito, H. Inoue, A simple method for evaluating the current in the cyclic voltammogram for reversible systems, J. Electroanal. Chem. 324 (1992) 397–404.
[7] R.G. Compton, C.E. Banks, Understanding Voltammetry, Imperial College Press, London, 2011.
[8] C. Batchelor-McAuley, E. Kätelhön, E.O. Barnes, R.G. Compton, E. Laborda, A. Molina, Recent advances in voltammetry, ChemistryOpen 4 (2015) 224–260.
[9] A.J. Bard, L.R. Faulkner, Electrochemical Methods — Fundamentals and Applications, Wiley, New York, 1980.
[10] G. Codina, G. Sanchez, A. Aldaz, Digital simulation of cyclic voltammetry on heterogeneous electrodes, Electrochim. Acta 36 (1991) 1129–1133.
[11] R.G. Compton, E. Laborda, K.R. Ward, Understanding Voltammetry: Simulation of Electrode Processes, Imperial College Press, London, 2014.
[12] Keith B. Oldham, Jan C. Myland, Modelling cyclic voltammetry without digital simulation, Electrochim. Acta. 56 (2011) 10612–10625.
[13] L.K. Bieniaz, Use of dynamically adaptive grid techniques for the solution of electrochemical kinetic equations Part 5. A finite-difference, adaptive space/time grid strategy based on a patch-type local uniform spatial grid refinement, for kinetic models in one-dimensional space geometry, J. Elecroanal. Chem. 481 (2000) 115–133.
[14] L.K. Bieniasz, Analysis of the applicability of the integral equation method in the theory of transient electroanalytical experiments for homogeneous reaction–diffusion systems: the case of planar electrodes, J. Elecroanal. Chem. 657(2011) 91–97.
[15] L.K. Bieniaz, High accurate, efficient, and automatic computation of reversible cyclic voltammograms, using double exponential formulas for numerical integration, J. Elecroanal. Chem. 808 (2018) 195–203.
[16] A. Ševčík, Oscillographic polarography with periodical triangular voltage, Collect. Czechoslov. Chem. Commun. 13 (1948) 349–377.
[17] J.E.B. Randles, A cathode ray polarograph. Part II.-the current-voltage curves, Trans. Faraday Soc. 44 (1948) 327–338.
[18] R.S. Nicholson, I. Shain, Theory of stationary electrode polarography. Single scan and cyclic methods applied to reversible, irreversible, and kinetic systems, Anal. Chem. 36 (1964) 706–723.
[19] H. Matsuda, Y. Ayabe, Zur Theorie der Randles-Sevčikschen Kathodenstrahl Palaeography, Z. Elektrochem. 59 (1955) 494–503. Berichte Der Bunsengesellschaft Für Phys. Chemie.
[20] R.S. Nicholson, Theory and application of cyclic voltammetry for measurement of electrode reaction kinetics, Anal. Chem. 37 (1965) 1351–1355.
[21] A. Samin, A one-dimensional stochastic approach to the study of cyclic voltammetry with adsorption effects, AIP Adv. 6 (2016), 055101.
[22] T. Berzins, P. Delahay, Oscillographic polarographic waves for the reversible deposition of metals on solid electrodes, J. Am. Chem. Soc. 75 (1953) 555–559.
[23] P. Delahay, Theory of irreversible waves in Oscillographic polarography, J. Am. Chem. Soc. 75 (1953) 1190–1196.
[24] D. Krulic, N. Fatouros, D. Liu, A complementary survey of staircase voltammetry with metal ion deposition on macroelectrodes, J. Electroanal. Chem. 754 (2015) 30–39.
[25] I. Atek, Semi-analytical modelling of linear scan voltammetric responses for soluble insoluble system: the case of metal deposition, J. Electroanal. Chem. 818 (2018) 35–43.
[26] I. Lavagnini, R. Antiochia, F. Magno, An extended method for the practical evaluation of the standard rate constant from cyclic voltammetric data, Electroanalysis 16 (2004) 505–506.
[27] J.G. Velasco, Determination of standard rate constants for electrochemical irreversible processes from linear sweep voltammograms, Electroanalysis 9 (1997) 880–882.
[28] K.B. Oldham, J. Electroanal. Chem 121 (1981) 341.
[29] A. Saila, Etude des systèmes électrochimiques quasi-réversibles par voltamperometrie a balayage linéaire et semi-intégration. Applications auX comportements de rhénium et dysprosium en milieuX de sels fondus, Univ. Badji Mokhtar, Annaba, 2010.
[30] A.M. Keightley, J.C. Myland, K.B. Oldham, P.G. Symons, Reversible cyclic voltammetry in the presence of product, J. Electroanal. Chem. 322 (1992) 25–54.
[31] M. Stieble, K. Jiittner, Surface blocking in the redoX system Pt/$[FeCN_6]^{-3}$, $[FeCN_6]^{-4}$, J. Electroanal. Chem. 290 (1990) 163–180.
[32] K. Winkler, The kinetics of electron transfer in $Fe(CN)_6^{4-/3-}$ redoX system on platinum standard-size and ultramicroelectrodes, J. Electroanal. Chem. 388 (1995) 151–159.
[33] W.J. BlaedeL, G.W. Schieffer, A hydrodynamic voltammetric study of the ferricyanide/ferrocyanide system with convective electrodes of platinum, gold, glassy carbon, carbon film, and boron carbide, J. Electroanal. Chem. 80 (1977) 259–271.
[34] M.H. Cheah, P. Cherne, Electrochemical oXidation of ferricyanide, Sci. Rep. 11 (2021) 23058.
[35] T. Singh, Cyclic voltammetry at the tubular electrode: Part II. Quasi-reversible and totally irreversible processes, J. Electroanal. Chem. 238 (1987) 33–41.
[36] L. Daruhbzi, K. Tokuda, Cyclic voltammetry for reversible redoX-electrode reactions in thin-layer cells with closely separated working and auXiliary electrodes of the same size, J. Electroanal. Chem 264 (1989) 77–89.
[37] M. Stieble, K. Jiittne, Surface blocking in the redoX system Pt/$[FeCN_6]^{-3}$, $[FeCN6]^{-4}$ An ac impedance study, J. Electroanal. Chem. 290 (1990) 163–180.
[38] D. Ball, J. Key, Introductory Chemistry –1st Canadian Edition, BCcampus, Victoria, B.C., 2014. Retrieved from, https://opentextbc.ca/introductorychemistry.
[39] J. Kwak, Revised reversible and totally sweep voltammetry irreversible zones for the linear at a planar electrode, Bull. Korean. Chem. Soc. 15 (1994) 57–63.
[40] W.C. Chen, H.M. Lin, C.A. Chang, Electrochemical study on screen-printed carbon electrodes with modification by iron nanoparticles in $Fe(CN)_6^{4-/3-}$ redoX system, Anal. Bioanal. Chem. 383 (2005) 532–538.
[41] L. Xiong, C. B-McAuley, K.R. Ward, C. Downing, R.S. Hartshorne, N.S. Lawrence, R. G. Compton, Voltammetry at graphite electrodes: the oXidation of hexacyanoferrate (II), (ferrocyanide) does not exhibit pure outer-sphere electron transfer kinetics and is sensitive to pre-exposure of the electrode to organic solvents, J. Electroanal. Chem. 661 (2011) 144–149.